Development of a Detailed Kinetic Model for the Oxidation of n -Butane in the Liquid Phase

M. Le, V. Warth, L. Giarracca, E. Moine, R. Bounaceur, R. Privat, Jean-Noël Jaubert, R. Fournet, P.-A. Glaude, B. Sirjean

Development of a Detailed Kinetic Model for the Oxidation *n*-Butane in the Liquid-Phase

M.D. Le[1], V. Warth[1], L. Giarracca[1], E. Moine[1], R. Bounaceur[1], R. Privat[1], J.-N. Jaubert[1], R. Fournet[1], P.-A. Glaude[1], B. Sirjean[1*]

[1] Laboratoire Réactions et Génie des Procédés, CNRS, Université de Lorraine

1 rue Grandville BP 20451 54001 Nancy Cedex, France

Corresponding author :

Baptiste Sirjean

Laboratoire Réactions et Génie des Procédés

1 rue Grandville BP 20451 54001 Nancy Cedex,

France

Email:baptiste.sirjean@univ-lorraine.fr

Abstract

The chemistry underlying liquid-phase oxidation of organic compounds, the main cause of their aging, is characterized by a free radical chain reaction mechanism. The rigorous simulation of these phenomena requires the use of detailed kinetic models that contain thousands of species and reactions. The development of such models for the liquid-phase remains a challenge as solvent-dependent thermo-kinetic parameters have to be provided for all the species and reactions of the model. Therefore, accurate and high-throughput methods to generate these data are required. In this work, we propose new methods to generate these data and we apply them for the development of a detailed chemical kinetic model for *n*-butane autoxidation, which is then validated against literature data. Our approach for model development is based on the work of Jalan et al. [*J. Phys. Chem. B*, **2013**, *117*, 2955–2970] who used Gibbs free energies of solvation ($\Delta_{solv}G(T)$) to correct the data of gas-phase kinetic model. In our approach, an equation of state is used to compute $\Delta_{solv}G$ as a function of temperature for all the chemical species in the mechanism. Currently, $\Delta_{solv}G(T)$ of free radicals cannot be computed with an equation of state and it was calculated for their parent molecule (H-atom added on the radical site). Theoretical calculations with implicit solvent model were performed to quantify the impact of this assumption and showed that it is acceptable for radicals in *n*-butane and probably in all *n*-alkanes. New rate rules were proposed for the most important reactions of the model, based on theoretical calculations and literature data. The developed detailed kinetic model for *n*-butane autoxidation is the first proposed in the literature and was validated against experimental data from the literature. Simulations showed that the main autoxidation products, *sec*-butyl hydroperoxides, and *2*-butanol are produced from H-abstractions from *n*-butane by *sec*-C_4H_9OO radicals, and the $C_4H_9OO + C_4H_9OO$ reaction, respectively. The uncertainty of the products ratio ('butanone + *2*-butanol' / '*2*-butoxy + *2*-butoxy') of the latter reaction remains high in the literature and our simulations suggest a 1:1 ratio in *n*-butane solvent.

1. Introduction

Liquid phase oxidation of organic compounds, also called autoxidation, is ubiquitous for all systems that are in contact with air. This natural phenomenon has negative effects on the stability of organic liquids, but it can also be desirable when it is controlled in industrial oxidation processes.[1] Autoxidation of liquid hydrocarbons is one of the main causes of fuel and lubricant aging that leads to deposit and gum formation.[2] The resistance of fuels to oxidation, called oxidation stability, is a crucial criterion for the usage of jet,[3] diesel[4], and gasoline[5] fuels as their autoxidation changes their chemical and physical structures and affects the fuel supply system and the engine efficiency. Linear and branched alkanes represent a major fraction of conventional petroleum fuels. The understanding of their autoxidation chemistry is therefore of primary importance. Oxidation stability of biofuels is also a key current research field as oxygenated molecules generally have lower oxidation stability compared to hydrocarbons.[6, 7]

Detailed chemical kinetic modeling of the autoxidation of fuels remains the only approach to provide fundamental insights on the underlying oxidation chemistry. However, the development of such kinetic models, rigorously adapted to the liquid phase, is scarce in the literature. Liquid phase oxidation occurs through a radical chain mechanism, similar to that found in gas phase oxidation, and involves hundreds to thousands of species and reactions.[8] In the gas phase, the development of detailed kinetic models for organic compound oxidation, mostly for combustion conditions, is well established.[9, 10] Combustion models of hydrocarbons contain hundreds of species and thousands of reactions with associated thermodynamic and kinetic data. Assuming that the gas phase behaves as a perfect gas, the thermo-kinetic data of a given compound are not influenced by those of another compound. However, in the liquid phase, thermo-kinetic data of solute become solvent-dependent and lead to an explosion of the number of necessary thermo-kinetic parameters. In fuel

autoxidation applications, the solvent is the fuel and a new set of fuel-specific thermodynamic and kinetic parameters must be provided for different fuels or their blends.

Software tools for the automatic generation of detailed combustion kinetic models make it possible to construct and manipulate such large mechanisms. These tools are also highly versatile as their development for a given organic compound (e.g., *n*-butane) implies that the combustion kinetic models of all the chemicals belonging to a same family (e.g., *n*-alkanes) can be generated. In the literature, several gas-phase kinetic model generators are available: RMG,[11] GENESYS,[12] MAMOX,[13] NetGen,[14] and EXGAS.[15, 16] Among all these automatic reaction mechanism generation codes, only RMG has been recently extended to liquid phase.

In a pioneering work, Green and co-workers proposed an extensible framework for capturing solvent effects in computer-generated kinetic models, and therefore extended the gas-phase kinetic models generated by RMG to liquid phase systems.[17] These authors demonstrated that solvent-adapted thermochemical data can be automatically computed by using Gibbs free energy of solvation[18-20] ($\Delta_{solv}G(T)$) corrections on generated gas-phase data. They achieved high-throughput calculations of $\Delta_{solv}G(T)$ for all the species of the mechanism using the Linear Solvation Energy Relationship (LSER) of Abraham and co-workers,[21, 22] combined to a group additivity method for the estimation of solute (species) descriptors used in the LSER.[22] This method could currently be applied for about 30 pure solvents. As shown by the authors, taking into account the temperature dependence on $\Delta_{solv}G$ in this LSER approach remains a challenge in the literature. In RMG, the approximation $\Delta_{solv}G(T) = \Delta_{solv}H^{\circ} - T\Delta_{solv}S^{\circ}$ is used to include first order temperature dependence. $\Delta_{solv}H^{\circ}$ is calculated using Mintz empirical correlation[23] (group additivity for solute descriptors) and $\Delta_{solv}S^{\circ}$ is estimated using scaled particle theory.[17] The calculation of $\Delta_{solv}G(T)$ for free radicals of the kinetic mechanism is achieved using empirical corrections to the solute descriptors of these species.

In RMG, the adaptation of gas-phase kinetic data to liquid-phase systems relies on corrections for diffusion limited bimolecular reactions, based on Smoluchowski theory.[24, 25] Automatic

estimation of this correction for a given reaction is achieved by calculating the species radii (McGowan scheme[26]) and diffusivities (Stokes–Einstein correlation and tabulated viscosities) in different solvents. High-throughput calculations of intrinsic solvent effects on rate constants remain a considerable challenge. In RMG, only a handful of reactions could be adapted to solution systems using gas-phase rate constants, solvent corrections, and theoretical calculations based on continuum dielectric models. This approach was shown to be promising to calculate liquid phase rate constants based on gas-phase data.[17]

In this work, we rely on the seminal work performed in RMG to explore alternative methods to capture solvent effects. These new approaches are applied to the development of a detailed kinetic model for the liquid phase oxidation (autoxidation) of *n*-butane. The kinetic model of autoxidation of *n*-butane, the simplest model molecule for larger *n*-alkane, is then validated against literature data. Once demonstrated, we aim at integrating this new methodology in our automatic generator of combustion kinetic models (EXGAS) for alkanes. In this study, the calculation of $\Delta_{solv}G(T)$ of all the species of the model is performed, for the first time in kinetic mechanisms, using an equation of state. This approach is compared with experimental data of the literature and theoretical calculations based on implicit solvent models. Gibbs free energies of solvation of all the free radicals of the mechanism are computed using theoretical chemistry. New reaction rate rules are proposed for the most sensitive reactions of the mechanism, based on literature review and theoretical calculations with implicit solvent models.

2. Detailed kinetic model development

A detailed chemical kinetic model was developed to simulate the oxidation of *n*-butane in the liquid phase. The starting point of the autoxidation model is the automatic generation of a gas-phase, low-temperature combustion, kinetic mechanism of *n*-butane, with EXGAS.[15]

Combustion models of hydrocarbons, generated with our EXGAS code, have been extensively validated in the literature.[27-31]

2.1. Calculation of Liquid Phase Thermochemical Data

Ideal gas thermochemical data for all the species of the mechanism are generated based on literature data or Benson group additivity method[32], implemented in our THERGAS code.[33] These data, expressed as NASA polynomials, are then corrected by $\Delta_{solv}G(T)$ using the equation of state UMR-PRU (Universal Mixing Rule Peng-Robinson UNIFAC).[34, 35] Solvation Gibbs energies of (infinitely) diluted solute in *n*-butane solvent are computed between 298 and 420 K. The input parameters of the UMR-PRU equation of state (EoS) are the pure component critical temperature and pressure (T_c, P_c) and acentric factor (ω) as well as the molecular group decomposition, this latter information being used by the model for quantifying binary interaction effects. For all the species of the kinetic mechanism, these parameters are either extracted from the DIPPR experimental database[36] or computed from group-contribution methods[37, 38] implemented in the ICAS software.[39] Recently, we compared experimental data of $\Delta_{solv}G(T)$ from the CompSol database[20] against predictions computed with UMR-PRU. A total of 9793 binary systems (solute–solvent combinations), which represents 53 237 data points, was studied. UMR-PRU was found to accurately predict these data with an average absolute deviation of 0.36 kcal/mol.[35] The level of accuracy was roughly preserved when all the pure-component input parameters (T_c, P_c, ω) of the EoS were estimated using group-contribution methods.

The calculation of $\Delta_{solv}G(T)$ for free radicals cannot be rigorously achieved using the UMR-PRU equation of state. In this work, we assume that $\Delta_{solv}G(T)$ for a free radical X• is equal to that of a parent molecule XH, i.e., the open-shell radical becomes a closed shell molecule by

adding a H-atom to the structure, on the free radical site. In order to verify this assumption, we calculated $\Delta_{solv}G(T)$ of free radicals and parent molecules using DFT calculations and implicit solvation. SMD[40] continuum solvation model calculations were performed using M06-2X/6-31+G(d) level of theory[41] with Gaussian 16.[42] Parameters for *n*-butane solvent calculations are given in Table S1.

We introduce here the validation of the calculation of $\Delta_{solv}G(T)$ of neutral molecules using SMD solvation model. Table 1 presents a comparison of computed $\Delta_{solv}G(T)$, using SMD implicit solvation model and UMR-PRU EoS, with the experimental data in *n*-butane solvent available in the CompSol database. For additional comparison, computations of $\Delta_{solv}G(T)$ with the conductor-like screening model for realistic solvation (COSMO-RS),[43] performed at the BP/TZVPD-FINE level, are also presented in Table 1.

Table 1: Comparison between experimental and computed $\Delta_{solv}G(T)$ (kcal mol^{-1}) for different solutes in *n*-butane solvent.

Solute	CompSol (T)	SMD (298 K)	COSMO-RS (T)	UMR-PRU (T)	T (K)
1,2-dimethylbenzene	-5.8	-5.9	-5.7	-5.5	290
1,3-dimethylbenzene	-5.7	-5.9	-5.6	-5.3	290
1,4-dimethylbenzene	-5.7	-5.9	-5.7	-5.3	290
styrene	-5.8	-5.8	-6.0	-5.9	270
toluene	-4.9	-5.5	-5.0	-4.7	290
benzene	-4.1	-5.1	-4.4	-4.1	290
propane	-2.2	-2.4	-1.8	-2.2	270
ethane	-1.3	-1.6	-1.1	-1.3	293
methane	-0.4	-0.1	-0.6	-0.5	210.9
methanol	-2.8	-1.8	-1.7	-3.1	273
Methyl tert-butyl ether	-3.4	-3.2	-3.3	-3.0	363.4
CO_2	-0.9	-0.1	-0.5	-0.8	273
H_2O	-0.4	-2.3	-0.5	-1.0	288.2
Mean Absolute Deviation (kcal/mol)		-0.17	0.12	0.06	

As already mentioned, the UMR-PRU equation of state is able to predict the experimental Gibbs free energies of solvation with a good accuracy, here in liquid *n*-butane. Theoretical calculations using implicit solvent models also show a good level of accuracy. It can be noted

that COSMO-RS calculations provide temperature-dependent $\Delta_{solv}G$ values while SMD values are computed at room temperature.

It is interesting to note that our method using the UMR-PRU equation of state is able to capture the temperature dependence of $\Delta_{solv}G$, with no additional approximation. Figure 1 presents a comparison of experimental and UMR-PRU computed $\Delta_{solv}G(T)$ data in liquid *n*-butane.

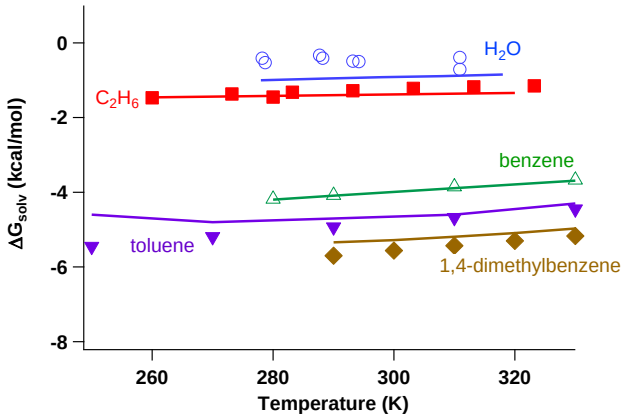

Figure 1: Comparison of experimental[20] (symbols) and computed (with UMR-PRU, lines) Gibbs free energies of different solutes in liquid *n*-butane.

UMR-PRU calculations of $\Delta_{solv}G(T)$ agree well with experimental data. It can be noted, that for *n*-butane solvent, and for this temperature range, the variations in Gibbs free energy of solvation remain linear and relatively small. In polar solvents, the variations of $\Delta_{solv}G$ with temperatures are not linear. It is worth noting that our approach based on an equation of state is able to capture this second-order behavior, as shown in Figure 2.

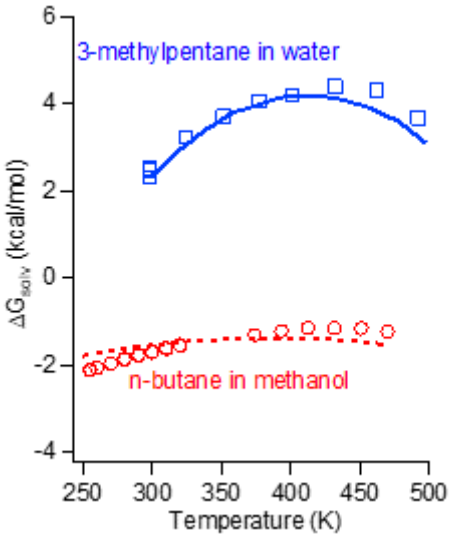

Figure 2: Comparison of experimental[20] (symbols) and computed (with UMR-PRU, lines) Gibbs free energies of different solutes in polar solvents (water and methanol).

Calculations based on an equation of state are able to rigorously include temperature dependence in Gibbs free energy of solvation. The accuracy of the computed results depends on the predictive capacity of the chosen EoS. Since our work focuses on the development of autoxidation models for *n*-alkanes, a more thorough discussion on the temperature dependence of solvation quantities in polar solvents is beyond the scope of this study.

The validation of the calculation of $\Delta_{solv}G(T)$ of neutral molecules using SMD solvation model has been shown. In our work, as mentioned earlier, $\Delta_{solv}G(T)$ for free radicals X• was computed for the parent molecule XH and was used to correct the gas-phase thermochemical data of the radical. To justify this approach, theoretical calculations performed at the M06-2X/6-31+G(d) level of theory with SMD implicit models were performed to quantify the differences in $\Delta_{solv}G$ between X• and XH, for all the free radicals of the mechanism. Computed results are given in Table 2.

Table 2: Comparison of computed Gibbs free energies of free radicals (X•) and parent molecules (XH) in *n*-butane solvent. M062X/6-31+G(d) level of theory with SMD implicit solvation model (kcal/mol).

Species	$\Delta_{solv}G$ (X•)	$\Delta_{solv}G$ (XH)	$\Delta_{solv}G$(XH) - $\Delta_{solv}G$(X•)
Primary radicals			

•CH_3	0.8	-0.1	-0.9
•CH_2OH	-0.9	-1.8	-0.9
•CH_2CHO	-2.6	-3.0	-0.4
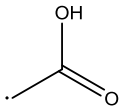	-3.6	-3.5	0.1
•C_2H_5	-1.2	-1.6	-0.4
n-•C_3H_7	-2.1	-2.4	-0.2
•C_3H_5	-1.9	-2.2	-0.3
n-•C_4H_9	-2.7	-3.0	-0.3
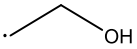	-2.5	-2.9	-0.4
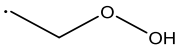	-3.1	-3.8	-0.7
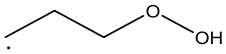	-3.8	-4.0	-0.2
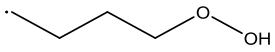	-4.4	-4.7	-0.3
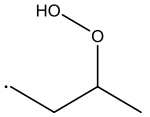	-4.1	-4.3	-0.2
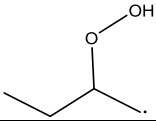	-4.2	-4.3	-0.1
Secondary radicals			
i-•C_3H_7	-2.4	-2.4	0.1
2-•C_4H_9	-3.1	-3.0	0.1
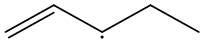	-2.9	-3.0	-0.1
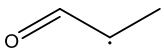	-4.0	-3.6	0.4
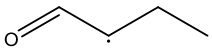	-4.4	-4.4	0.0
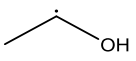	-2.5	-2.9	-0.4
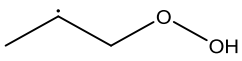	-3.3	-4.0	-0.7
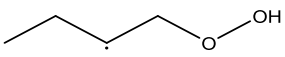	-4.8	-4.7	0.1
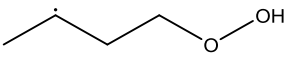	-4.8	-4.7	0.1

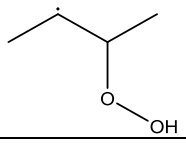	-4.4	-4.3	0.1
Vinyl and carbonyl radicals			
•CHO	-0.5	-1.2	-0.7
•C_2H_3	-0.7	-1.1	-0.4
•CHCO	-1.2	-1.6	-0.4
•C_2H	0.1	-1.0	-1.1
$CH_3C(•)O$	-2.2	-3.0	-0.9
$CH_3OC(•)O$	-1.2	-2.9	-1.7
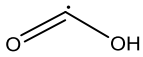	-2.1	-3.2	-1.1
Alkoxy radicals			
HO•	-1.8	-2.3	-0.5
$CH_3O•$	-1.7	-1.8	-0.1
$CH_3CH_2O•$	-2.9	-2.9	0.0
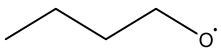	-4.3	-4.2	0.1
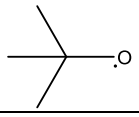	-3.7	-3.8	-0.1
Peroxy radicals			
HOO•	-2.3	-2.6	-0.3
$CH_3OO•$	-2.3	-2.3	0.0
$CH_3CH_2OO•$	-3.5	-3.8	-0.3
$CH_3CH_2CH_2OO•$	-4.2	-4.0	0.2
$CH_3CH_2CH_2CH_2OO•$	-4.8	-4.7	0.1
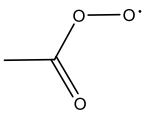	-3.8	-3.6	0.2
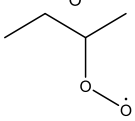	-4.4	-4.3	0.1

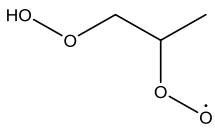	-5.4	-5.4	0.0
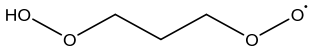	-5.7	-5.5	0.2
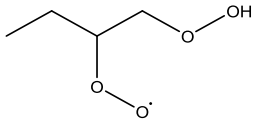	-5.4	-5.5	-0.1
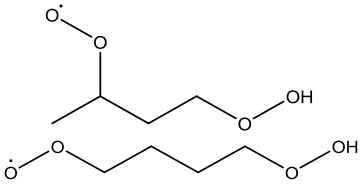	-5.6	-5.6	0.0
	-6.1	-6.1	0.0
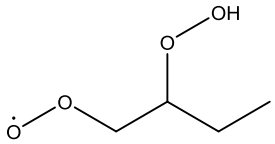	-5.4	-5.5	-0.1
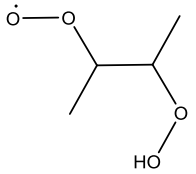	-5.3	-5.4	-0.1
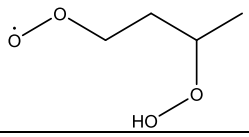	-5.6	-5.6	0.0

Calculations results presented in Table 2 show that, in *n*-butane solvent, the difference in Gibbs free energies of solvation of free radicals and parent molecules are very small. The assumption $\Delta_{solv}G(X\bullet) = \Delta_{solv}G(XH)$ used in our kinetic model is therefore appropriate. It can be noted that the mean absolute deviation of $\Delta_{solv}G(XH) - \Delta_{solv}G(X\bullet)$ for the 50 free radicals considered here is -0.3 kcal/mol. Overall, the Gibbs free energies of solvation of free radicals are slightly lower than that of parent molecules. This behavior is more pronounced for small radicals (< 2 heavy atoms) and for those of the primary radical and vinyl/carbonyl groups of Table 2. For other groups of radicals in Table 2, $\Delta_{solv}G(XH) - \Delta_{solv}G(X\bullet)$ is generally negligible.

We expect this conclusion to apply also for other *n*-alkanes, but also to all other hydrocarbons which have a similar dielectric constant (ε). This assumption is confirmed in Figure 3 that

presents the evolution of computed $\Delta_{solv}G(C_2H_5OOH)$ and $\Delta_{solv}G(C_2H_5OO\bullet)$ in different solvents of increasing ε.

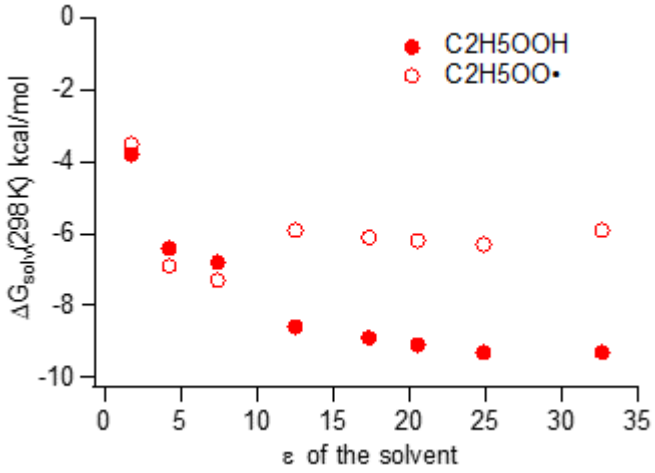

Figure 3: Gibbs free energies of solvation of C_2H_5OOH and $C_2H_5OO\bullet$ in different solvents, computed at the M062X/6-31+G(d) level of theory with SMD solvation model. Solvents and their dielectric constants[42]: *n*-butane (ε = 1.77), diethyl ether (ε = 4.24), tetrahydrofuran (ε = 7.43), 1-hexanol (ε = 12.51), 1-butanol (ε = 17.33), 1-propanol (ε = 20.52), ethanol (ε = 24.85), methanol (ε = 32.61).

Computed results presented in Figure 3 show that the differences in $\Delta_{solv}G$ for $C_2H_5OO\bullet$ radical and its parent molecule remain small for solvents with dielectric constants below ≈ 8. Since ε values for linear, branched and cyclic alkanes and alkenes are around 2 and those for aromatics are around 2.3, the computation of $\Delta_{solv}G(T)$ of the parent molecule with UMR-PRU that is further used for free radicals seems a reasonable assumption for hydrocarbons. For solvents with higher ε values, this assumption leads to ≈3.0 kcal/mol differences that may not be negligible.

2.2. Liquid Phase Kinetic Data

Kinetic data used in the *n*-butane autoxidation kinetic model are based on gas-phase data and new liquid phase correlations from literature or theoretical calculations. In this work, liquid-phase adapted rate constants deriving from literature experimental data or theoretical calculations were used for the most sensitive reactions of the model, while gas-phase kinetic data were used for all the other reactions. Gas-phase kinetic data were generated with EXGAS.[15, 16] Unimolecular rate constants remained unchanged, while bimolecular rate

constants were corrected for diffusive limits (see 2.2.1). The target validation data for the autoxidation kinetic model are the experimental data measured by Mill et al.[44] In these experiments, these authors used *di-tert*-butyl peroxide (tBu_2O_2) as initiator. Thus, we included the initiation mechanism of *di-tert*-butyl peroxide in our model. The most important features of the developed mechanism are presented below.

2.2.1. Diffusion correction on bimolecular rate constants

Diffusive limits in the liquid phase were considered using a diffusion rate constant (k_{diff}) that was combined to the intrinsic liquid-phase constant ($k_{int,liq}$) yielding an effective rate (k_{eff}) constant for a bimolecular reaction A+B ⇆ (A-B) → *Products* as: [16]

$$k_{eff} = \frac{k_{diff} \times k_{int,liq}}{k_{diff} + k_{int,liq}}$$

with k_{diff} calculated using:

$$k_{diff} = 4\pi \cdot (r_A + r_B) \cdot (D_A + D_B)$$

where r_A and r_B are the radii of reactants A and B and D_A and D_B are their diffusivity coefficients. D_{ij}, the diffusion coefficient of a solute *i* in a solvent *j*, is calculated using the Stoke-Einstein equation:

$$D_{ij} = \frac{k_B T}{6\pi\eta_j r_i}$$

where η_j is the viscosity of the solvent *j* and r_i is the molecular radius of the solute *i*.

In this work, we used the temperature-dependent experimental viscosity of liquid *n*-butane from DIPPR database.[45] Molecular radii of solutes were obtained from the volume parameter R_k of UNIFAC, which is available in our approach as a parameter of the UMR-PRU EoS:

$$r_i = 3.18 \cdot 10^{-10} \times \left(\sum_k \nu_k^{(i)} R_k \right)^{1/3}$$

Where r_i is in meter and $\nu_k^{(i)}$ denotes the occurrence of group k in molecule (i).

A similar approach is used in RMG, but with a method based on McGowan method for the calculation of molecular radii.[17] For most sensitive reactions of the model, $k_{int,liq}$ is a rate constant computed with theoretical chemistry. For non-sensitive reactions $k_{int,liq}$ is assumed to be similar to the gas-phase rate constant generated by EXGAS. k_{diff} was computed for all bimolecular reactions of the mechanism, but, because of the low viscosity of *n*-butane, diffusion constants are always negligible for all the reactions of the mechanism (for both direct and reverse directions). Kinetic data for which diffusion corrections were noticeable are given in Table 3.

Table 3 : Diffusion corrected rate constant in the kinetic model.

Reaction	**k_{eff}**			**k_{diff} (400K)**
	A	n	E_a	**cm^3 $mole^{-1}$ s^{-1}**
n-C_4H_{10} + OH = *sec*-C_4H_9 + H_2O	8.40E+06	1.94	-662.6	1.69 10^{14}
sec-C_4H_9 + O_2 = *sec*-C_4H_9OO	9.89E+17	-2.038	0.0	1.64 10^{14}
sec-C_4H_9OH + OH = $CH_3C(OH)CH_2CH_3$ + H_2O	1.17E+12	0.0	-349.5	1.72 10^{14}
$CH_3C(OH)CH_2CH_3$ + O_2 = $CH_3C(OO)(OH)CH_2CH_3$	1.77E+18	-2.219	0.0	1.65 10^{14}
$CH_3COCH_2CH_3$ + OH = $CH_3COCHCH_3$ + H_2O	4.48E+12	0.0	562.4	1.69 10^{14}

Rate expression: $k = AT^n \exp\left(\frac{-E_a}{RT}\right)$ in cm^3, mol, cal, K, s units.

From Table 3, it can be seen that diffusion rate constants are high. Indeed, the effective rate constants are lowered by, at most 3% at 400 K, compared to rate constants without diffusion corrections. For example, $k_{int,liq}$(400 K) and k_{diff} (400K) of *sec*-C_4H_9 + O_2 = *sec*-C_4H_9OO are, respectively, 5.31 10^{12} and 1.64 10^{14} cm^3 mol^{-1} s^{-1}. These values lead to k_{eff}(400 K) = 5.15 10^{12} cm^3 mol^{-1} s^{-1}.

2.2.2. Initiations and β-scissions

Bimolecular initiations with O_2 involve reactions R1-R2, where two radicals, *n*-butyl (*n*-C_4H_9) and *sec*-butyl (*sec*-C_4H_9) radicals, are produced. Initial C-C bond fissions in *n*-butane (R3-R4), yielding methyl (CH_3), ethyl (C_2H_5), and *n*-propyl (*n*-C_3H_7) radicals were also included. EXGAS rate rules for gas-phase kinetic were adopted for these reactions.

n-C_4H_{10} + O_2 = *sec*-C_4H_9 + HO_2 (R1)

n-C_4H_{10} + O_2 = *n*-C_4H_9 + HO_2 (R2)

n-C_4H_{10} = CH_3 + *n*-C_3H_7 (R3)

n-C_4H_{10} = C_2H + C_2H_5 (R4)

In the conditions of low temperature of liquid-phase oxidation, only C-C β-scissions of butyl isomer radicals were considered. Via these reactions (R5-R6), *n*-butyl radical produces ethylene (C_2H_4) and ethyl radical while *sec*-butyl radical forms propene (C_3H_6) and methyl radical.

sec-C_4H_9 = CH_3 + C_3H_6 (R5)

n-C_4H_9 = C_2H_5 + C_2H_4 (R6)

For these reactions, gas-phase kinetic data were used.

2.2.3. Addition with oxygen and oxidation

n-Butyl and *sec*-butyl radicals additions on O_2 yield *n*-butyl peroxy (*n*-C_4H_9OO) radical and *sec*-butyl peroxy (*sec*-C_4H_9OO) radical respectively (R7-R8).

In the model, the addition on O_2 of the butyl isomer radicals competes with the oxidation reactions. These butyl radicals can be oxidized by oxygen to form 1-butene (*1*-C_4H_8) and 2-butene (*2*-C_4H_8) via reactions (R9-R11). These reactions were included as, according to Mill et al.[44], they account for the experimental observation of traces of *n*-butenes during *n*-butane liquid-phase oxidation.

$$sec\text{-}C_4H_9 + O_2 = sec\text{-}C_4H_9OO \quad (R7)$$

$$n\text{-}C_4H_9 + O_2 = n\text{-}C_4H_9OO \quad (R8)$$

$$sec\text{-}C_4H_9 + O_2 = 1\text{-}C_4H_8 + HO_2 \quad (R9)$$

$$sec\text{-}C_4H_9 + O_2 = 2\text{-}C_4H_8 + HO_2 \quad (R10)$$

$$n\text{-}C_4H_9 + O_2 = 1\text{-}C_4H_8 + HO_2 \quad (R11)$$

Gas-phase kinetic data generated by EXGAS were used for these reactions.

2.2.4. H-abstraction reactions

H-atom abstractions are the principal consumption route of *n*-butane during its liquid-phase oxidation. These reactions involve the reaction of *n*-butane with radicals that are significantly produced at low temperatures. In our work, the following radicals were included in H-abstraction reactions: hydroxyl (OH), hydroperoxyl (HO_2), methyl (CH_3), methoxy (CH_3O), methyl peroxy (CH_3OO), ethyl (C_2H_5), ethoxy (C_2H_5O), ethyl peroxy (C_2H_5OO), *sec*-butoxy (*sec*-C_4H_9O), *n*-butyl peroxy (*n*-C_4H_9OO), and *sec*-butyl peroxy (*sec*-C_4H_9OO).

In the experiments of Mill et al.[44], *2*-butanol was found as one of the major primary products, while *1*-butanol was not observed. Mill et al. showed that *2*-butanol is formed through a H-atom abstraction by *sec*-butoxy radical from *n*-butane, and that *sec*-butoxy comes from the decomposition of *sec*-butyl hydroperoxide. These authors showed that *n*-butyl hydroperoxide was not significantly produced.

$$n\text{-}C_4H_{10} + OH = sec\text{-}C_4H_9 + H_2O \quad (R10)$$

$$n\text{-}C_4H_{10} + OH = n\text{-}C_4H_9 + H_2O \quad (R11)$$

$$n\text{-}C_4H_{10} + HO_2 = sec\text{-}C_4H_9 + H_2O_2 \quad (R12)$$

$$n\text{-}C_4H_{10} + HO_2 = n\text{-}C_4H_9 + H_2O_2 \quad (R13)$$

$$n\text{-}C_4H_{10} + CH_3 = sec\text{-}C_4H_9 + CH_4 \quad (R14)$$

$$n\text{-}C_4H_{10} + CH_3 = n\text{-}C_4H_9 + CH_4 \quad (R15)$$

n-C_4H_{10} + CH_3O = *sec*-C_4H_9 + CH_3OH (R16)

n-C_4H_{10} + CH_3O = n-C_4H_9 + CH_3OH (R17)

n-C_4H_{10} + CH_3OO = *sec*-C_4H_9 + CH_3OOH (R18)

n-C_4H_{10} + CH_3OO = n-C_4H_9 + CH_3OOH (R19)

n-C_4H_{10} + C_2H_5 = *sec*-C_4H_9 + C_2H_6 (R20)

n-C_4H_{10} + C_2H_5 = n-C_4H_9 + C_2H_6 (R21)

n-C_4H_{10} + C_2H_5O = *sec*-C_4H_9 + C_2H_5OH (R22)

n-C_4H_{10} + C_2H_5O = n-C_4H_9 + C_2H_5OH (R23)

n-C_4H_{10} + C_2H_5OO = *sec*-C_4H_9 + C_2H_5OOH (R24)

n-C_4H_{10} + C_2H_5OO = n-C_4H_9 + C_2H_5OOH (R25)

n-C_4H_{10} + *sec*-C_4H_9O = *sec*-C_4H_9 + *sec*-C_4H_9OH (R26)

n-C_4H_{10} + *sec*-C_4H_9O = n-C_4H_9 + *sec*-C_4H_9OH (R27)

n-C_4H_{10} + *sec*-C_4H_9OO = *sec*-C_4H_9 + *sec*-C_4H_9OOH (R28)

n-C_4H_{10} + *sec*-C_4H_9OO = n-C_4H_9 + *sec*-C_4H_9OOH (R29)

n-C_4H_{10} + n-C_4H_9OO = *sec*-C_4H_9 + n-C_4H_9OOH (R30)

n-C_4H_{10} + n-C_4H_9OO = n-C_4H_9 + n-C_4H_9OOH (R31)

The rate constants of H-atom abstractions by OH, HO_2, CH_3, C_2H_5 followed the rate rules of EXGAS. H-atom abstractions by alkoxy and peroxy radicals are the main propagation reactions, and we established new reaction rate rules based on theoretical calculations of rate constants of R26 and R28.

The liquid-phase rate constants for these reactions were computed using the following method:

- calculation of the gas-phase high-pressure limit rate constants (k_{gas}) based on electronic structure calculations (at the CBS-QB3 level of theory[46]) and transition state theory with rigid rotor harmonic oscillator approach for all vibrational modes, internal

rotations excepted. The latter modes were treated using 1D-HR method[47, 48] based on relaxed scans performed at the B3LYP/6-311G(d,p) level of theory. Quantum tunnelling was included using an Eckart potential. k_{gas} were determined using our in-house code ThermRot.[47]

- Computed k_{gas} is adapted to solvent environment using Gibbs free energies of solvation for transition state structures and reactants. $\Delta_{solv}G$ of reactants and transition states were computed at the M06-2X/6-31+G(d) level of theory with the SMD solvation model. The intrinsic liquid-phase rate constant ($k_{int,\ liq}$) of a reaction is obtained from:

$$k_{int,liq} = k_{gas} \times \exp\left(-\frac{\Delta\Delta G^{\ddagger}_{solv}}{RT}\right)$$

where $\Delta\Delta G^{\ddagger}_{solv}$ is the Gibbs free energy of solvation of activation (difference between the transition state structure and the reactant).

The calculated rate constants of reactions R26 and R28 are given in Table 4 and compared to the gas-phase rate constant generated by EXGAS. Cartesian coordinates of reactants and transition state structures are given in Table S2.

Table 4: Comparison of k_{EXGAS} (gas-phase rate constant of EXGAS) and $k_{int,liq}$ (calculated) of H-atom abstractions of *n*-butane by *sec*-butoxy radical (R26) and sec-butyl peroxide radical (R28).

Reaction	k_{EXGAS}				$k_{int,liq}$			
	A	n	E_a	Value at 400 K	A	n	E_a	Value at 400 K
R26	2.90E+11	0.0	4500	1.01E+09	1.46E+10	0.0	3890	1.09E+08
R28	6.00E+12	0.0	17500	1.64E+03	1.45E+12	0.0	17765	2.85E+02

Rate expression: $k = AT^n \exp\left(\frac{-E_a}{RT}\right)$ in cm^3, mol, cal, K, s units.

In the typical temperature range (300-500 K) of liquid-phase oxidation, the EXGAS rate constants of reactions R26 and R28 are about 10 and 4 times, respectively, higher than the corresponding calculated liquid rate constants. These factors 10 and 4 were used to correct

gas-phase rate constants generated by EXGAS. In the model, the rate constants of H-atom abstractions from *n*-butane by CH_3O (R16), C_2H_5O (R22), producing *sec*-butyl radical, are based on analogies with R26 and those by CH_3OO (R18), C_2H_5OO (R24), *n*-C_4H_9OO (R30) also yielding *sec*-butyl radical are based on analogies with R28.

2.2.5. Disproportionations

Disproportionations are termination reactions. In the model, these reactions involve peroxy radicals. Butyl peroxy reacts with HO_2 as ROO + HO_2 → ROOH + O_2. Kinetic parameters of these reactions follow EXGAS rate rules defined as $k = 2.0 \times 10^{11} \times \exp(1300/RT)$ in cm^3, mol, cal, K, s.

Another type of disproportionation, specific to condensed phases, was considered in the model: the self-termination reactions of *sec*-butyl peroxy radicals. As discussed by Mill et al.[44], these reactions could happen in two ways, R32 producing *sec*-butoxy (*sec*-C_4H_9O) radical and O_2 or R33, also known as the Russell mechanism,[49] yielding *sec*-butanol (*sec*-C_4H_9OH) and butanone ($CH_3COCH_2CH_3$).

sec-C_4H_9OO + *sec*-C_4H_9OO → *sec*-C_4H_9O + *sec*-C_4H_9O + O_2 (R32)

sec-C_4H_9OO + *sec*-C_4H_9OO → $CH_3COCH_2CH_3$ + *sec*-C_4H_9OH + O_2 (R33)

Self-termination reactions of *sec*-butyl peroxy have been experimentally investigated by Howard et al.[50] The rate constant of the global reaction *sec*-C_4H_9OO + *sec*-C_4H_9OO → *Products* was reported as $k_{global} = 1.0 \times 10^{12} \times \exp(-2700/RT)$ in cm^3, mol, cal, K, s. The ratio k_{R32}/k_{R33} was estimated between 1 and 2 by Mill et al.[44] In our model, the k_{R32}/k_{R33} ratio is defined as 1/1 and each rate constant take a value of $k = 0.25 \times 10^{11} \times \exp(-2700/RT)$ in cm^3, mol, cal, K, s. The sensivity of the k_{R32}/k_{R33} ratio value on the simulation results will be discussed in details in the section dedicated to the kinetic analysis of the simulations.

2.2.6. Secondary mechanism

This section describes important features in the development of sub-mechanisms of molecules formed in the primary mechanism, whose oxidation reactions are not included in the C_0-C_4 reaction basis. The sub-mechanism of the *di-tert*-butyl peroxide initiator is also presented.

Decompositions of hydroperoxides

In oxidation, the unimolecular decomposition of hydroperoxides (ROOH) play a crucial role on reactivity as it generates two free radicals (RO and OH). In our model, the rate constant of decomposition of *sec*-butyl hydroperoxide (R34) is k = 1.67 x 10^7 x exp(-24041/RT) in cm^3, mol, cal, K, s. This rate constant deduced from experimental data reported in the review of Brandrup et al.[51], which includes data for *sec*-C_4H_9OOH decomposition in toluene.

The decomposition of *sec*-C_4H_9OOH yields *sec*-butoxy radical (*sec*-C_4H_9O), which can decompose by β-scission to form C_2H_5 radical and acetaldehyde (R35). The rate constant of this reaction, k = 1.10 x 10^{12} x exp(-12811/RT) in cm^3, mol, cal, K, s, was adapted from the experimental gas-phase rate constant measured by Falgayrac et al.[52] The correction was based on the experimental profiles of specific minor products (ethanol, acetaldehyde) produced during liquid *n*-butane auto-oxidation.[44]

sec-C_4H_9OOH = *sec*-C_4H_9O + OH (R34)

sec-C_4H_9O = C_2H_5 + CH_3CHO (R35)

2-butanol sub-mechanism

2-butanol was found as one of the major primary products of *n*-butane liquid-phase oxidation experiments.[44] The sub-mechanism of 2-butanol includes H-atom abstractions (R36-R38) of this compound by the main active radicals: OH, HO_2, and *sec*-C_4H_9OO. As the C-H bond energy on the α-site of the hydroxyl group is the weakest among all C-H bonds in 2-butanol,[53] the main product of H-atom abstractions from 2-butanol is $CH_3C•H(OH)CH_2CH_3$ (α-hydroxy-sec-butyl) radical. To limit the size of the mechanism, we assumed that this H-atom abstraction was preponderant over all the other H-atom abstractions from 2-butanol. Rate

parameters were adopted from the kinetic model of combustion of 2-butanol developed by Sarathy et al.[53]

sec-C_4H_9OH + OH = $CH_3C(OH)CH_2CH_3$ + H_2O (R36)

sec-C_4H_9OH + HO_2 = $CH_3C(OH)CH_2CH_3$ + H_2O_2 (R37)

sec-C_4H_9OH + *sec*-C_4H_9OO = $CH_3C(OH)CH_2CH_3$ + *sec*-C_4H_9OOH (R38)

In the sub-mechanism, the α-hydroxy-sec-butyl radical is oxidized by O_2 to form butanone in two steps: addition on O_2 (R39) ($k = 1.77 \times 10^{18} \times T^{-2.22}$ in cm^3, mol, cal, K, s, per EXGAS rate rule) followed by HO_2 radical elimination (R40). The kinetic parameters of this reaction were calculated using the same theoretical method as the one described in section 2.2.3 for R26 and R28. The computed rate constant of R40 is $k = 5.53 \times 10^{11} \times T^{0.34} \times \exp(-11830/RT)$ in s^{-1}.

di-tert-butyl peroxide sub-mechanism

The rate constant for the unimolecular decomposition of *di-tert*-butyl peroxide (tBu_2O_2) was chosen as $k = 2.0 \times 10^{19} \times \exp(-43746/RT)$ in cm^3, mol, cal, K, s, based on a regression analysis using liquid-phase experimental data reported in the review of Brandrup et al.[51]

tBu_2O_2 = tert-C_4H_9O + tert-C_4H_9O (R41)

Once formed via reaction R41, *tert*-butoxy (*tert*-C_4H_9O) radical either produced *tert*-butanol (*tert*-C_4H_9OH) by H-atom abstractions from *n*-butane (R42-R43) or decomposes by β-scission (R44).

n-C_4H_{10} + *tert*-C_4H_9O = *n*-C_4H_9 + *tert*-C_4H_9OH (R42)

n-C_4H_{10} + *tert*-C_4H_9O = *sec*-C_4H_9 + *tert*-C_4H_9OH (R43)

tert-C_4H_9O = CH_3COCH_3 + CH_3 (R44)

The rate constants of reactions (R42-R43) are based on analogies with H-atom abstractions of other alkoxy radicals discussed in section 2.1.3. The estimated rate constant of R44 is based on the gas phase rate constant ($k_{gas} = 1.00 \times 10^{14} \times \exp(-14460/RT)$ in cm^3, mol, cal, K, s)

measured by Fittschen et al.[54] adapted to a solvent environment with an empirical factor (k_{gas} A factor multiplied by 0.1) determined from simulations of experimental *tert*-butanol and acetone profiles.

A sub-mechanism for *tert*-butanol decomposition was also included in the model. H-atom abstractions from a methyl group of *tert*-butanol were included (R44-R46). The $(CH_3)_2COCH_2$ radical produced is then consumed by addition on O_2 (R47), followed by a lumped decomposition reaction of the peroxy radical yielding acetone (CH_3COCH_3), formaldehyde (HCHO), and OH radical.

$$tert\text{-}C_4H_9OH + OH = (CH_3)_2COCH_2 + H_2O \quad (R44)$$

$$tert\text{-}C_4H_9OH + HO_2 = (CH_3)_2COCH_2 + H_2O_2 \quad (R45)$$

$$tert\text{-}C_4H_9OH + sec\text{-}C_4H_9OO = (CH_3)_2COCH_2 + sec\text{-}C_4H_9OOH \quad (R46)$$

$$(CH_3)_2COCH_2 + O_2 = (CH_3)_2COCH_2OO \quad (R47)$$

$$(CH_3)_2COCH_2OO \rightarrow CH_3COCH_3 + HCHO + OH \quad (R48)$$

Kinetic parameters of all reactions of *tert*-butanol sub-mechanism are adapted from the *tert*-butanol combustion kinetic model developed by Sarathy et al.[53]

3. Results and discussion

3.1. Kinetic model validation

The detailed kinetic model developed for the autoxidation of *n*-butane contains 131 species and 716 reactions. It has been validated against species profiles measured by Mill et al.[44] These authors investigated liquid *n*-butane oxidation in presence of *di-tert*-butyl peroxide (tBu_2O_4), used as an initiator, in a closed reactor whose temperature was held constant during each manipulation. Temperatures varied from 100°C to 125°C. Table 5 summarizes the experimental conditions. For different experiments performed at the same temperature, initial concentrations of *n*-butane were held constant in the experiments. Dissolved oxygen

concentrations were calculated using computed Henry's law constant with COSMO-RS: at 100°C and 125°C, $[O_2] \approx 8 \times 10^{-6}$ mol/cm^3.

Table 5: Experimental conditions of *n*-butane autoxidation.[44]

Experiment #	T (K)	[*n*-Butane] (mol/cm^3)	[*di-tert*-Butyl peroxide] (mol/cm^3)	Reaction time (min)	Conversion of *n*-butane (%)
1	373	8.12 x 10^{-3}	3.84 x 10^{-5}	284	0.07
2	373	8.12 x 10^{-3}	2.25 x 10^{-6}	1124	0.07
3	373	8.12 x 10^{-3}	4.18 x 10^{-5}	1439	0.13
4	373	8.12 x 10^{-3}	6.32 x 10^{-5}	1462	0.32
5	373	8.12 x 10^{-3}	6.59 x 10^{-5}	4339	0.95
6	398	7.04 x 10^{-3}	2.91 x 10^{-6}	178	0.09
7	398	7.04 x 10^{-3}	3.32 x 10^{-5}	178	0.66

Simulations were performed using a model of homogeneous liquid batch reactor (constant T, P, and V), developed in-house and based on the Chemkin II library.[55] Oxygen concentration was kept constant during the simulations.

Figure 4.a. and 4.b. present the simulated and experimental conversion of *n*-butane as a function of reaction time and initial concentration of tBu_2O_2. It was experimentally found that the conversion of *n*-butane increased linearly with the product of reaction time and initial concentration of tBu_2O_2 et constant temperature. This observation is well reproduced by the developed kinetic model.

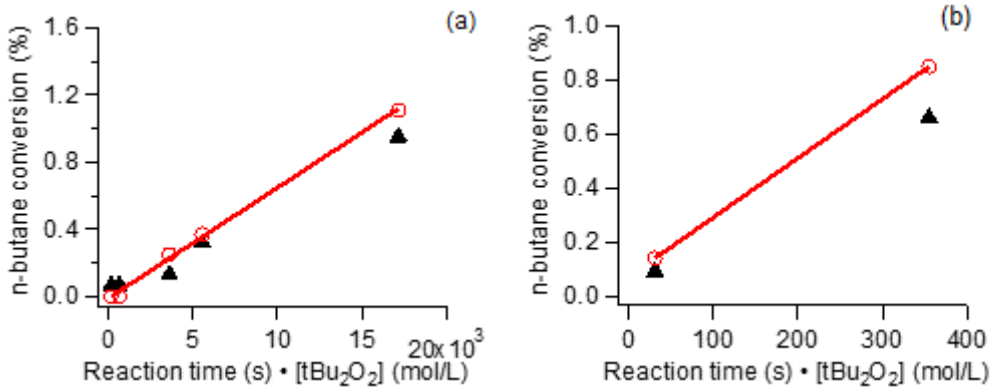

Figure 4: Conversion of *n*-butane measured in liquid-phase oxidation experiments in a closed reactor.[44] (a) T = 100 °C. (b) = 125 °C. Filled symbols: experiments. Open symbols: simulations. Lines are a linear fit of the simulations points and are drawn to guide the eye.

Figure 5 shows the simulation of products of *n*-butane autoxidation, for different conversions of *n*-butane.

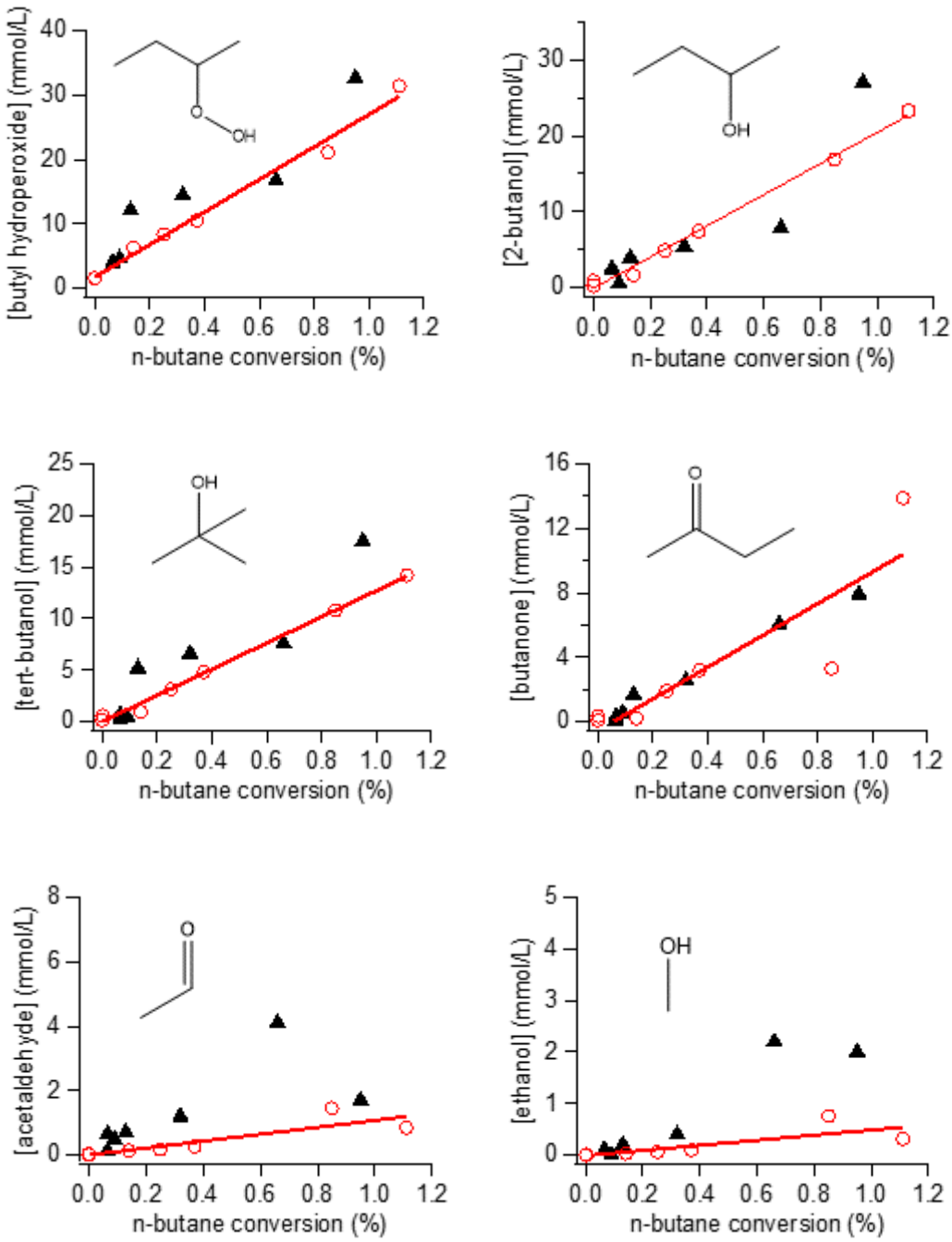

Figure 5: Evolution of *n*-butane liquid-phase oxidation products as a function of *n*-butane conversion. Experimental conditions include experiments at 100 and 125 °C. Filled symbols: experiments performed by Mill et al.[44] Open symbols: simulations. Lines are a linear fit of the simulations points and are drawn to guide the eye.

Butyl hydroperoxides and *sec*-butanol are the major primary products of *n*-butane autoxidation. *tert*-Butanol formation is due to the use of *di-tert*-butyl peroxide as an initiator. Butanone, acetaldehyde, and ethanol were also measured in small amounts. At low conversion (< 1%), oxidation products including butyl hydroperoxides, *sec*-butanol, *tert*-butanol, and butanone increase almost linearly with the conversion of *n*-butane. The kinetic model simulates quantitively the formation of these products. Minor products including acetaldehyde and ethanol are underestimated by the model within a factor of 3 at the maximum concentration point. The temperature-dependence of the formation of these products are well characterized by the developed model (see Figure S1 to discriminate experimental points at 100 and 125°C). Overall, the simulations agree well with experimental results upon adjustments of the rate parameters of R32, R33, R35 and R44, which are new estimations of these kinetic data in liquid *n*-butane.

One question that would be raised is whether a *n*-butane gas-phase kinetic model developed for low-temperature combustion could reasonably simulate the liquid-phase oxidation of *n*-butane. To clarify this point, simulations were done using the *n*-butane gas-phase kinetic model developed by Cord et al.[54]. The sub-mechanism of decomposition of *di-tert*-butyl peroxide (tBu_2O_2), used in our liquid-phase model, was incorporated in the model of Cord et al.[54]. While the *n*-butane conversion was always below 1% in the conditions of the experiments of Mill et al.[42], the simulated *n*-butane conversion, under the same conditions, usingy the gas-phase model of Cord et al.[54] was between 39 and 100% depending on the conditions. The experiment-simulation disagreement confirms the importance of the development of a kinetic model specifically dedicated to liquid-phase oxidation.

3.2. Kinetic analyses of *n*-butane autoxidation

3.2.1. Reaction flux analysis

Rate of production (ROP) analyses were carried out in the condition of the experiment #5 of Mill et al.,[44] listed in Table 5. This experiment was conducted at 100 °C and the conversion of *n*-butane was about 1%. Figure 6 presents the main reaction pathway of *n*-butane liquid-phase oxidation at the examined condition.

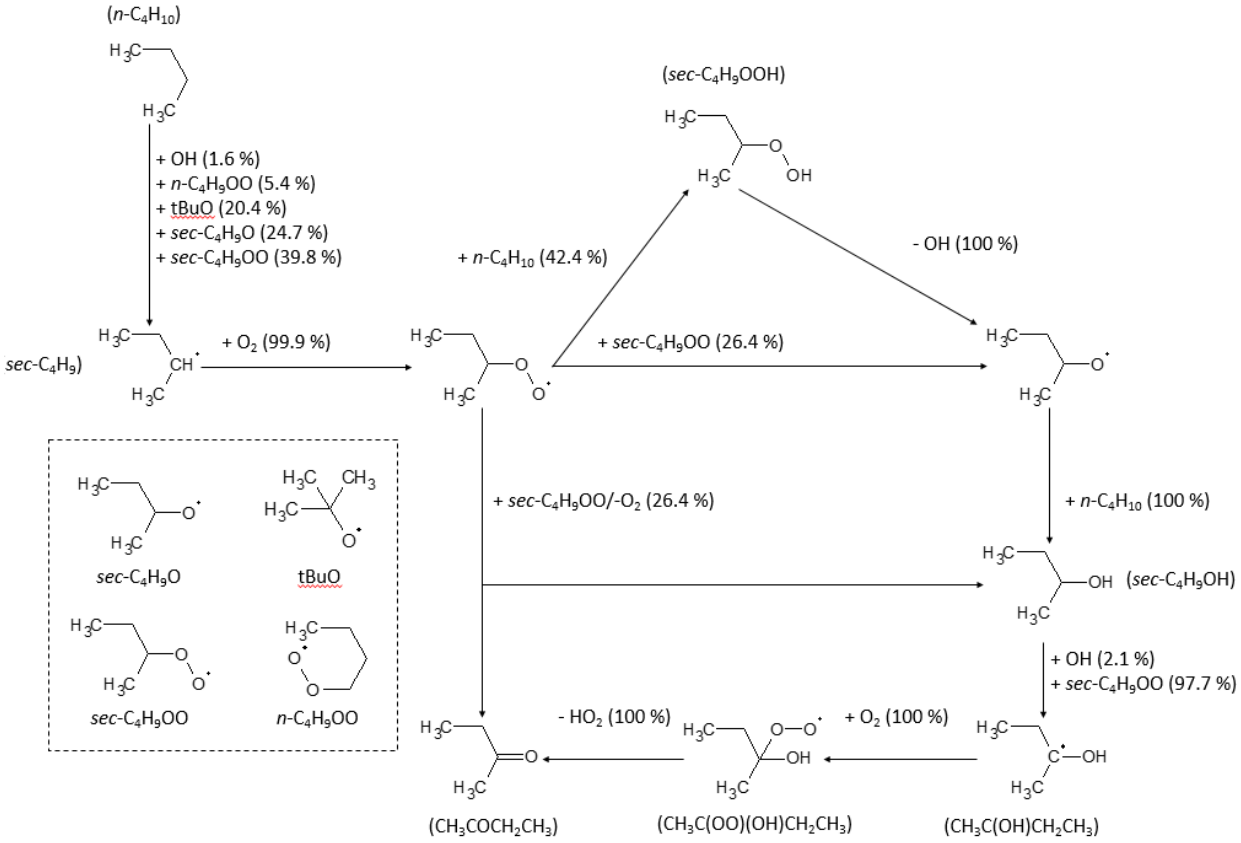

Figure 6: Reaction pathways of *n*-butane oxidation in the liquid phase, at 100 °C, in the presence of di-*tert*-butyl peroxide.

The main consumption fluxes of *n*-butane are H-atomabstractions by *sec*-butyl peroxy (39.8%), *sec*-butoxy (24.7%), *tert*-butoxy (20.4%), *n*-butyl peroxy (5.4%) and OH (1.6%) radicals, all yielding *sec*-butyl radical. The latter radical solely forms *sec*-butyl peroxy radical (*sec*-C_4H_9OO) through addition on O_2. Nearly half of the consumption flux of *sec*-butyl peroxy radical (42.4%) yields *sec*-butyl hydroperoxide via H-atom abstractions from *n*-butane. The remaining consumption routes of this radical involve the self-termination reactions *sec*-C_4H_9OO + *sec*-C_4H_9OO that produce *2*-butanol and butanone by the Russell

mechanism, and *sec*-butoxy radicals. *sec*-Butyl hydroperoxide is a degenerate branching agent, which entirely decomposes into two radicals, *sec*-butoxy, and OH radicals. This reaction is the most important reaction governing the liquid-phase reactivity of *n*-butane as it transforms a neutral molecule into two reactive radicals. *sec*-Butanol is produced by both self-termination reactions of *sec*-butyl peroxide radical and H-atom abstraction of *n*-butane by *sec*-butoxy radical. This alcohol is then oxidized into butanone by some successive reactions: H-atom abstractions, addition on O_2, and elimination of HO_2.

3.2.2. Sensivity analyses

Sensitivity analyses have been performed on the conversion of *n*-butane in the same condition used in the above reaction flux analysis. To do this, the A-factor of each reaction rate constant was multiplied by a factor of ten. For each reaction rate modification, a simulation was conducted to determine the conversion (X_i) of *n*-butane. The sensitivity coefficient (τ_i) of each reaction was then calculated as follows:

$$\tau_i = \frac{X_i - X_0}{X_0} \times 100\ \%$$

X_0 represents the simulated conversion of *n*-butane with the original unmodified model. A positive sensitivity coefficient means the considered reaction showing a promoting effect on the liquid-phase reactivity of *n*-butane. Conversely, a negative coefficient indicating an inhibiting effect of the considered reaction on the liquid-phase reactivity of *n*-butane. Figure 7 presents the result of the sensitivity analyses. Considering *n*-butane sub-mechanism, the reactions having promoting effect are H-atom abstraction from *n*-butane by butyl peroxy radicals (R28, R29, R30), the decomposition of the *sec*-butyl hydroperoxide (R34), the disproportionation of *sec*-butyl peroxy radical producing butoxy radicals (R32). The reaction R28 has the highest promoting effect. The termination reaction of *sec*-butyl peroxy radical producing *sec*-butanol and butanone (R33) was found inhibiting. Several reactions of the sub-

mechanism of the initiator *di-tert*-butyl peroxide are sensitive. The decomposition of *di-tert*-butyl peroxide (R41) presents a promoting effect while the decomposition of *tert*-butoxy radical (R44) shows an inhibiting effect.

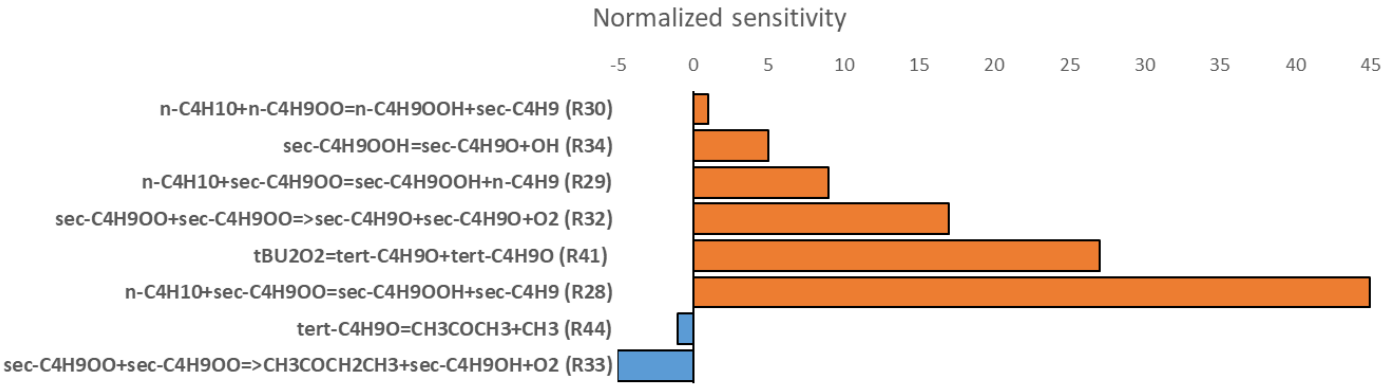

Figure 7: Sensitivity analyses on the conversion of *n*-butane in the liquid-phase oxidation at 373 K.

Reaction flux analysis and sensitivity analyses highlighted some important reactions governing *n*-butane liquid-phase reactivity: H-atom abstractions by sec-butyl peroxide and *sec-butoxy* radicals, decomposition of *sec*-butyl hydroperoxide, self-termination of *sec*-butyl peroxide radicals. The H-atom abstractions were calculated by theoretical chemistry. The rate constant of *sec*-butyl hydroperoxide decomposition was determined thanks to experimental data from the literature. The most significant uncertainty in these major reaction pathways resides in the kinetic data of the self-termination of *sec*-butyl peroxy radicals. As discussed in section 2.2.4, the self-termination of *sec*-butyl peroxy radicals occurs through the Russell mechanism (R32) and (R33).

$$sec\text{-}C_4H_9OO + sec\text{-}C_4H_9OO \rightarrow sec\text{-}C_4H_9O + sec\text{-}C_4H_9O + O_2 \qquad (R32)$$

$$sec\text{-}C_4H_9OO + sec\text{-}C_4H_9OO \rightarrow CH_3COCH_2CH_3 + sec\text{-}C_4H_9OH + O_2 \qquad (R33)$$

The rate constant of the global reaction sec-C_4H_9OO + sec-C_4H_9OO → *Products* was reported as $k_{global} = 1.00 \times 10^{12} \times \exp(-2700/RT)$ in cm^3, mol, cal, K, s by Mill et al.[44] or $k_{global} = 1.26 \times 10^{10} \times \exp(-1100/RT)$ by Furimsky et al.[55]. The uncertainty in the kinetic parameters of the

termination of *sec*-C_4H_9OO is remarkable (a factor of 10) at low temperatures (100-125 °C), which requires further investigations. In our model, a rate constant $k = 0.25 \times 10^{11} \times \exp(-2700/RT)$ in cm^3, mol, cal, K, s was proposed for R32 and R33. This rate constant is close to the value reported by Furimsky et al.[55] at low temperatures (100-125 °C). It should be noted that the branching ratio defined as $a = k_{R32} / k_{R33}$ has not been explicitly determined. Mill et al.[44] estimated that this ratio could be between 1 and 2. In the present work, this ratio was set to 1. We investigated the effect of the ratio *a* varying from 0.5 to 2 on the simulation of liquid-phase reactivity of *n*-butane. Table 6 presents the absolute reaction rates k_{R32}, k_{R33} corresponding to each examined *a* values.

Table 6: Rate constants of self-termination reactions (R32, R33) of *sec*-butyl peroxy corresponding to different branching ratio $a = k_{R32} / k_{R33}$

a	0.5	1.0	1.5	2
$\mathbf{k_{R32}}$	$0.17\times10^{11} \times e^{-2700/RT}$	$0.25 \times 10^{11} \times e^{-2700/RT}$	$0.30 \times 10^{11} \times e^{-2700/RT}$	$0.33 \times 10^{11} \times e^{-2700/RT}$
$\mathbf{k_{R33}}$	$0.33\times10^{11} \times e^{-2700/RT}$	$0.25 \times 10^{11} \times e^{-2700/RT}$	$0.20 \times 10^{11} \times e^{-2700/RT}$	$0.17 \times 10^{11} \times e^{-2700/RT}$

The influence of different values of the ratio *a* on the conversion of *n*-butane, in the conditions of the experiments of Mill et al.[44] is presented in Figure 8.

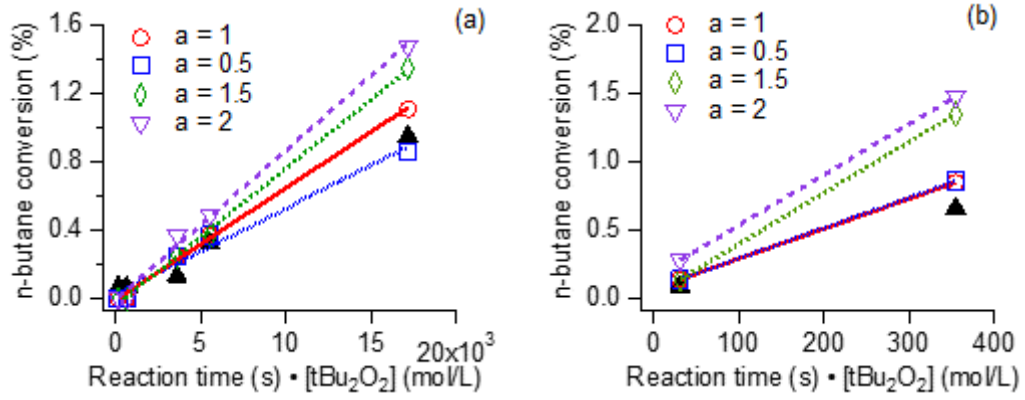

Figure 8: Impact of the branching ratio *a* of self-termination reactions of *sec*-butyl peroxy radicals on the simulation of *n*-butane conversion in the liquid-phase. Filled symbols: experiments; open symbols: simulations. (a) T = 100 °C. (b) T = 125 °C. Lines are a linear fit of the simulations points and are drawn to guide the eye.

The simulated conversion of *n*-butane increases with the branching ratio *a*. By enhancing *a*, the self-reaction of *sec*-butyl peroxy radicals proceeds toward the reaction R_{32}, favouring the formation of *sec*-butoxy radicals. These radicals contribute to the consumption of *n*-butane by H-atom abstractions and increase the reactivity. Decreasing *a* favors reaction R33 leads to stable molecule (butanone and 2-butanol) and inhibits the reactivity of liquid *n*-butane. Figure 7 also confirms that the use of $a = 1$ in our model is appropriate to simulate the *n*-butane conversion measured by Mill et al.[44]

Conclusions

A first detailed kinetic model for *n*-butane oxidation in the liquid phase has been developed using a methodology. Our approach is based on solvent-adapted-corrections that are applied to models designed for the gas-phase oxidation. Thermodynamic data are corrected to the liquid-phase using Gibbs free energies of solvation computed with the UMR-PRU equation of state. The use of this EoS was shown to give accurate $\Delta_{solv}G$ as a function of temperature for a large number of solvents.[35] The calculation of $\Delta_{solv}G(T)$ for all the free radicals of the mechanism was performed using the value computed for a parent molecule (H-atom added to the radical center). The error induced by this assumption was systematically quantified for all radicals by theoretical calculations at the M06-2X/6-31+G(d) level of theory and using the SMD continuum solvation model. The theoretical calculations showed that the differences in $\Delta_{solv}G$ between the radical and its parent molecule remains small in *n*-butane solvent, for all types of radicals involvedin the autoxidation mechanism. It was also shown that this "parent molecule" assumption probably remains acceptable for solvent with a dielectric constant up to ≈8. Consequently, this approach can probably be applied to all alkanes, alkenes, aromatic, and most ether solvents. For more polar solvents, the "parent molecule" assumption to compute free radical Gibbs free energies may be too imprecise, and an alternative approach or corrections need to be proposed. Theoretical calculations of rate constants were also

performed for the most important H-atom abstractions from *n*-butane, by *sec*-C_4H_9OO and *sec*-C_4H_9O radicals. Diffusive limits on bimolecular rate constants were found to be negligible in *n*-butane solvent. Several new rate rules were established based on theoretical results, literature data or simulation results and were used to develop the first detailed kinetic model of *n*-butane autoxidation of the literature. The model was validated against experimental data of the literature and is able to simulate the conversion of *n*-butane and the main products formed during its autoxidation at low conversion. Kinetic analyses show that a classical chain mechanism leading to the formation of hydroperoxides by H-atom abstraction from *n*-butane by sec-C_4H_9OO peroxy radicals is the major consumption route. The self-reaction sec-C_4H_9OO + sec-C_4H_9OO is also shown to play a major role in the reaction fluxes. The uncertainty of the kinetic parameters and the products ratio ('butanone + 2-butanol' / '*sec*-butoxy + *sec*-butoxy') of this reaction remains high and deserves more studies. Using experimental data as a constrain on simulations, we found that the products ratio is 1:1 in *n*-butane solvent. The methods proposed in this study can be applied to develop detailed kinetic models of autoxidation for any linear alkanes of interest. In particular, thermodynamic corrections to adapt gas-phase data to the liquid-phase, based on an equation of state, can be used as a fast high-throughput method for automatic generation of a kinetic model.

Supplemental material

Parameters of SMD calculations of n-butane solvent, cartesian coordinates of optimized geometries used in rate constant calculations, experimental products profiles discriminated for two temperatures, and the detailed kinetic model are given in supplemental material.

Acknowledgements

This work was financially supported by the ANR BioACe project, grant ANR-18-CE05-002 of the French National Research Agency. High performance computing

resources were provided by the EXPLOR center hosted by the University of Lorraine. This work was also granted access to the HPC resources of IDRIS under the allocation 2019-A0010807249 made by GENCI.

References

1. Suresh, A. K.; Sharma, M. M.; Sridhar, T., Engineering aspects of industrial liquid-phase air oxidation of hydrocarbons. *Ind. Eng. Chem. Res.* **2000,** *39* (11), 3958-3997.
2. Chatelain, K.; Nicolle, A.; Ben Amara, A.; Catoire, L.; Starck, L., Wide range experimental and kinetic modeling study of chain length impact on n-alkanes autoxidation. *Energy Fuels* **2016,** *30* (2), 1294-1303.
3. Hazlett, R. N., *Thermal oxidation stability of aviation turbine fuels*. ASTM International: West Conshohocken, PA, 1991.
4. Batts, B.; Fathoni, A. Z., A literature review on fuel stability studies with particular emphasis on diesel oil. *Energy Fuels* **1991,** *5* (1), 2-21.
5. Pradelle, F.; Braga, S. L.; Martins, A. R. F.; Turkovics, F.; Pradelle, R. N., Gum formation in gasoline and its blends: A review. *Energy Fuels* **2015,** *29* (12), 7753-7770.
6. Jain, S.; Sharma, M., Stability of biodiesel and its blends: a review. *Renew. Sustain. Energy Rev.* **2010,** *14* (2), 667-678.
7. El-Sayah, Z.; Glaude, P.-A.; Fournet, R.; Sirjean, B. *Comparison of the Effects of Different Biofuels on the Oxidation Stability of a Hydrocarbon Fuel*; 0148-7191; SAE Technical Paper: 2020.
8. Denisov, E. T.; Afanas' ev, I. B., *Oxidation and antioxidants in organic chemistry and biology*. CRC Press: Boca Raton, Fl, 2005.
9. Battin-Leclerc, F.; Blurock, E.; Bounaceur, R.; Fournet, R.; Glaude, P.-A.; Herbinet, O.; Sirjean, B.; Warth, V., Towards cleaner combustion engines through groundbreaking detailed chemical kinetic models. *Chem. Soc. Rev.* **2011,** *40* (9), 4762-4782.
10. Van de Vijver, R.; Vandewiele, N. M.; Bhoorasingh, P. L.; Slakman, B. L.; Seyedzadeh Khanshan, F.; Carstensen, H. H.; Reyniers, M. F.; Marin, G. B.; West, R. H.; Van Geem, K. M., Automatic mechanism and kinetic model generation for gas- and solution- phase processes: a perspective on best practices, recent advances, and future challenges. *Int. J. Chem. Kinet.* **2015,** *47* (4), 199-231.
11. Gao, C. W.; Allen, J. W.; Green, W. H.; West, R. H., Reaction Mechanism Generator: Automatic construction of chemical kinetic mechanisms. *Comput. Phys. Commun.* **2016,** *203*, 212-225.
12. Vandewiele, N. M.; Van Geem, K. M.; Reyniers, M.-F.; Marin, G. B., Genesys: Kinetic model construction using chemo-informatics. *Chem. Eng. J.* **2012,** *207*, 526-538.
13. Ranzi, E.; Faravelli, T.; Gaffuri, P.; Sogaro, A., Low-temperature combustion: automatic generation of primary oxidation reactions and lumping procedures. *Combust. Flame* **1995,** *102* (1-2), 179-192.
14. Broadbelt, L. J.; Stark, S. M.; Klein, M. T., Computer generated pyrolysis modeling: on-the-fly generation of species, reactions, and rates. *Ind. Eng. Chem. Res.* **1994,** *33* (4), 790-799.
15. Warth, V.; Stef, N.; Glaude, P.; Battin-Leclerc, F.; Scacchi, G.; Côme, G., Computer-aided derivation of gas-phase oxidation mechanisms: application to the modeling of the oxidation of n-butane. *Combust. Flame* **1998,** *114* (1-2), 81-102.
16. Buda, F.; Bounaceur, R.; Warth, V.; Glaude, P.-A.; Fournet, R.; Battin-Leclerc, F., Progress toward a unified detailed kinetic model for the autoignition of alkanes from C4 to C10 between 600 and 1200 K. *Combust. Flame* **2005,** *142* (1-2), 170-186.
17. Jalan, A.; West, R. H.; Green, W. H., An extensible framework for capturing solvent effects in computer generated kinetic models. *J. Phys. Chem. B* **2013,** *117* (10), 2955-2970.
18. Jalan, A.; Ashcraft, R. W.; West, R. H.; Green, W. H., Predicting solvation energies for kinetic modeling. *Annu. Rep. Prog. Chem., Sect. C: Phys. Chem.* **2010,** *106*, 211-258.
19. Ben-Naim, A. Y., *Solvation thermodynamics*. Springer Science & Business Media: New York, USA, 2013.

20. Moine, E.; Privat, R.; Sirjean, B.; Jaubert, J.-N., Estimation of Solvation Quantities from Experimental Thermodynamic Data: Development of the Comprehensive CompSol Databank for Pure and Mixed Solutes. *J. Phys. Chem. Ref. Data* **2017,** *46* (3), 033102.
21. Abraham, M. H., Application of solvation equations to chemical and biochemical processes. *Pure Appl. Chem.* **1993,** *65* (12), 2503-2512.
22. Platts, J. A.; Butina, D.; Abraham, M. H.; Hersey, A., Estimation of molecular linear free energy relation descriptors using a group contribution approach. *J. Chem. Inf. Comput. Sci.* **1999,** *39* (5), 835-845.
23. Mintz, C.; Clark, M.; Burton, K.; Acree Jr, W. E.; Abraham, M. H., Enthalpy of solvation correlations for gaseous solutes dissolved in benzene and in alkane solvents based on the Abraham model. *QSAR Comb. Sci.* **2007,** *26* (8), 881-888.
24. Collins, F. C.; Kimball, G. E., Diffusion-controlled reaction rates. *J. Colloid Sci.* **1949,** *4* (4), 425-437.
25. Smoluchowski, M., Sur le chemin moyen parcouru par les molécules d'un gaz et sur son rapport avec la théorie de la diffusion. *Bulletin de l'Ac. des Sc. de Cracovie* **1906,** *1*, 202 - 213.
26. Abraham, M. H.; McGowan, J., The use of characteristic volumes to measure cavity terms in reversed phase liquid chromatography. *Chromatographia* **1987,** *23* (4), 243-246.
27. Cord, M.; Sirjean, B.; Fournet, R.; Tomlin, A.; Ruiz-Lopez, M.; Battin-Leclerc, F., Improvement of the modeling of the low-temperature oxidation of n-butane: study of the primary reactions. *J. Phys. Chem. A* **2012,** *116* (24), 6142-6158.
28. Cord, M.; Husson, B.; Lizardo Huerta, J. C.; Herbinet, O.; Glaude, P.-A.; Fournet, R.; Sirjean, B.; Battin-Leclerc, F.; Ruiz-Lopez, M.; Wang, Z., Study of the low temperature oxidation of propane. *J. Phys. Chem. A* **2012,** *116* (50), 12214-12228.
29. Herbinet, O.; Husson, B.; Serinyel, Z.; Cord, M.; Warth, V.; Fournet, R.; Glaude, P.-A.; Sirjean, B.; Battin-Leclerc, F.; Wang, Z., Experimental and modeling investigation of the low-temperature oxidation of n-heptane. *Combust. Flame* **2012,** *159* (12), 3455-3471.
30. Schönborn, A.; Le, M. D.; Fournet, R.; Glaude, P.-A.; Warth, V.; Sirjean, B., Auto-ignition control using an additive with adaptable chemical structure. Part I: Development of a kinetic model for 1, 3-cyclohexadiene and 1, 3, 5-hexatriene combustion. *Combust. Flame* **2019,** *205*, 466-483.
31. Schönborn, A.; Le, M. D.; Fournet, R.; Glaude, P.-A.; Warth, V. r.; Sirjean, B., Autoignition Control Using an Additive with Adaptable Chemical Structure. Part 2. Development of a PRF Kinetic Model Including 1, 3-Cyclohexadiene Mechanism and Simulations of Ignition Control. *Energy Fuels* **2019,** *33* (12), 12704-12713.
32. Benson, S. W., *Thermochemical kinetics: methods for the estimation of thermochemical data and rate parameters*. Wiley: 1968.
33. Muller, C.; Michel, V.; Scacchi, G.; Côme, G.-M., THERGAS: a computer program for the evaluation of thermochemical data of molecules and free radicals in the gas phase. *J. Chim. Phys.* **1995,** *92*, 1154-1178.
34. Voutsas, E.; Louli, V.; Boukouvalas, C.; Magoulas, K.; Tassios, D., Thermodynamic property calculations with the universal mixing rule for EoS/GE models: Results with the Peng–Robinson EoS and a UNIFAC model. *Fluid Phase Equilib.* **2006,** *241* (1-2), 216-228.
35. Moine, E.; Privat, R.; Jaubert, J.-N.; Sirjean, B.; Novak, N.; Voutsas, E.; Boukouvalas, C., Can we safely predict solvation Gibbs energies of pure and mixed solutes with a cubic equation of state? *Pure Appl. Chem.* **2019**.
36. Rowley, R.; Wilding, W.; Oscarson, J.; Yang, Y.; Giles, N., DIPPR 801 property database, Software Package. *New York: Design Institute for Physical Property Data, American Institute of Chemical Engineers* **2009**.
37. Marrero, J.; Gani, R., Group-contribution based estimation of pure component properties. *Fluid Phase Equilib.* **2001,** *183*, 183-208.

38. Joback, K. G.; Reid, R. C., Estimation of pure-component properties from group-contributions. *Chem. Eng. Commun.* **1987,** *57* (1-6), 233-243.
39. Gani, R.; Hytoft, G.; Jaksland, C.; Jensen, A. K., An integrated computer aided system for integrated design of chemical processes. *Comput. Chem. Eng.* **1997,** *21* (10), 1135-1146.
40. Marenich, A. V.; Cramer, C. J.; Truhlar, D. G., Universal solvation model based on solute electron density and on a continuum model of the solvent defined by the bulk dielectric constant and atomic surface tensions. *J. Phys. Chem. B* **2009,** *113* (18), 6378-6396.
41. Zhao, Y.; Truhlar, D. G., The M06 suite of density functionals for main group thermochemistry, thermochemical kinetics, noncovalent interactions, excited states, and transition elements: two new functionals and systematic testing of four M06-class functionals and 12 other functionals. *Theor. Chem. Acc.* **2008,** *120* (1-3), 215-241.
42. Frisch, M. J.; Trucks, G. W.; Schlegel, H. B.; Scuseria, G. E.; Robb, M. A.; Cheeseman, J. R.; Scalmani, G.; Barone, V.; Petersson, G. A.; Nakatsuji, H.; al., e. *Gaussian 16 Rev. C.01*, Wallingford, CT, 2016.
43. Klamt, A.; Jonas, V.; Bürger, T.; Lohrenz, J. C., Refinement and parametrization of COSMO-RS. *J. Phys. Chem. A* **1998,** *102* (26), 5074-5085.
44. Mill, T.; Mayo, F.; Richardson, H.; Irwin, K.; Allara, D. L., Gas-and liquid-phase oxidations of butane. *J. Am. Chem. Soc.* **1972,** *94* (19), 6802-6811.
45. Wilding, W. V.; Rowley, R. L.; Oscarson, J. L., DIPPR® Project 801 evaluated process design data. *Fluid Phase Equilib.* **1998,** *150*, 413-420.
46. Montgomery Jr, J. A.; Frisch, M. J.; Ochterski, J. W.; Petersson, G. A., A complete basis set model chemistry. VI. Use of density functional geometries and frequencies. *J. Chem. Phys.* **1999,** *110* (6), 2822-2827.
47. Lizardo-Huerta, J.; Sirjean, B.; Bounaceur, R.; Fournet, R., Intramolecular effects on the kinetics of unimolecular reactions of β-HOROO˙ and HOQ˙ OOH radicals. *PCCP* **2016,** *18* (17), 12231-12251.
48. Vansteenkiste, P.; Van Neck, D.; Van Speybroeck, V.; Waroquier, M., An extended hindered-rotor model with incorporation of Coriolis and vibrational-rotational coupling for calculating partition functions and derived quantities. *J. Chem. Phys.* **2006,** *124* (4), 044314.
49. Russell, G. A., Deuterium-isotope effects in the autoxidation of aralkyl hydrocarbons. mechanism of the interaction of peroxy radicals1. *J. Am. Chem. Soc.* **1957,** *79* (14), 3871-3877.
50. Howard, J.; Bennett, J., The self-reaction of sec-alkylperoxy radicals: a kinetic electron spin resonance study. *Can. J. Chem.* **1972,** *50* (14), 2374-2377.
51. Brandrup, J.; Immergut, E. H.; Grulke, E. A.; Abe, A.; Bloch, D. R., *Polymer handbook*. Wiley New York: 1999; Vol. 89.
52. Falgayrac, G.; Caralp, F.; Sokolowski-Gomez, N.; Devolder, P.; Fittschen, C., Rate constants for the decomposition of 2-butoxy radicals and their reaction with NO and O 2. *PCCP* **2004,** *6* (16), 4127-4132.
53. Sarathy, S. M.; Vranckx, S.; Yasunaga, K.; Mehl, M.; Oßwald, P.; Metcalfe, W. K.; Westbrook, C. K.; Pitz, W. J.; Kohse-Höinghaus, K.; Fernandes, R. X., A comprehensive chemical kinetic combustion model for the four butanol isomers. *Combust. Flame* **2012,** *159* (6), 2028-2055.
54. Fittschen, C.; Hippler, H.; Viskolcz, B., The β C–C bond scission in alkoxy radicals: thermal unimolecular decomposition of t-butoxy radicals. *PCCP* **2000,** *2* (8), 1677-1683.
55. Kee, R. J.; Rupley, F. M.; Miller, J. A. *Chemkin-II: A Fortran chemical kinetics package for the analysis of gas-phase chemical kinetics*; Sandia National Lab.(SNL-CA), Livermore, CA (United States): 1989.

TOC Graphic

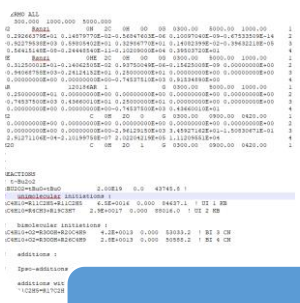

Gas Phase Oxidation Kinetic Model

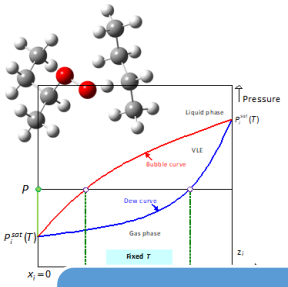

Equation of State

DFT

Implicit solvation model

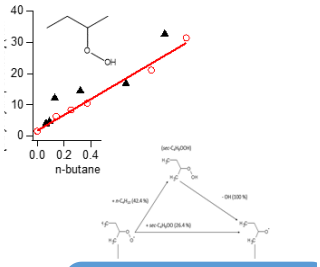

Solvent adapted thermokinetic data

Simulations of experiments and analyses